The Cryosphere Discuss., 7, 6001–6042, 2013
www.the-cryosphere-discuss.net/7/6001/2013/
doi:10.5194/tcd-7-6001-2013

The Cryosphere Discussions
Open Access

A 10 yr record of black carbon and dust from Mera Peak ice core (Nepal): variability and potential impact on Himalayan glacier melting

P. Ginot[1,2,3], M. Dumont[4], S. Lim[2,3], N. Patris[5], J.-D. Taupin[5], P. Wagnon[6,7], A. Gilbert[2,3], Y. Arnaud[6], A. Marinoni[8,9], P. Bonasoni[8,9], and P. Laj[2,3]

[1]IRD/Univ. Grenoble Alpes/CNRS/Univ. Savoie/INPG/IFSTTAR/CNRM, Observatoire des Sciences de l'Univers de Grenoble (OSUG) UMS222, Grenoble, 38041, France
[2]Univ. Grenoble Alpes, Laboratoire de Glaciologie et Géophysique de l'Environnement (LGGE) UMR5183, Grenoble, 38041, France
[3]CNRS, Laboratoire de Glaciologie et Géophysique de l'Environnement (LGGE) UMR5183, Grenoble, 38041, France
[4]Météo France/CNRS, Centre d'Etude de la Neige (CEN) CNRM-GAME UMR 3589, 38041, Grenoble, France
[5]IRD/CNRS/UM1/UM2, HydroSciences Montpellier (HSM) UMR5569, Montpellier, 34095, France
[6]IRD/UGA/CNRS/INPG, Laboratoire d'étude des Transferts en Hydrologie et Environnement (LTHE) UMR5564, Grenoble 38041, France

[7]ICIMOD, GPO Box 3226, Kathmandu, Nepal
[8]CNR – Institute for Atmospheric Sciences and Climate, Bologna, Italy
[9]EvK2CNR, Bergamo, 24126, Italy

Received: 4 November 2013 – Accepted: 2 December 2013 – Published: 13 December 2013

Correspondence to: P. Ginot (patrick.ginot@ird.fr)

Published by Copernicus Publications on behalf of the European Geosciences Union.

Abstract

A shallow ice core of the southern flank of Nepalese Himalaya range was extracted from the summit of Mera Peak at 6376 m a.s.l. in Nepal. From this core, we have reconstructed the seasonal deposition fluxes of dust and refractory black carbon (rBC) since 1999. This archive presents well preserved seasonal cycles based on monsoonal precipitation pattern. According to the seasonal precipitation regime, 80 % of the annual precipitation between June and September, we estimated the surface snow concentrations evolution for these aerosols. The analyzes reveals that mass fluxes are a few orders of magnitude higher for dust ($10.2 \pm 2.5\,g\,m^{-2}\,yr^{-1}$) that for rBC ($3.2 \pm 1.2\,mg\,m^{-2}\,yr^{-1}$).These data were used to simulate the surface snow albedo changes with time and the induced potential melting related to these impurities. The potential melting associated to joint dust and rBC can reach $660\,kg\,m^{-2}\,yr^{-1}$, and $220\,kg\,m^{-2}\,yr^{-1}$ for rBC only under some assumptions. Compared to the melting rate measured by mass and energy balance at 5400 m a.s.l. on Mera glacier, close to the equilibrium altitude, the impact of rBC represents less than 7 % of annual potential melting while the joint contribution of dust and rBC of the surface melting represents a maximum 18 %. Furthermore, over this 10 yr time span, the fluxes variability in the ice core signal is rather reflecting the variability of the monsoon signal than that of emission intensity.

1 Introduction

Emissions of long-lived greenhouse gases, short-lived reactive trace gases and particles from natural and anthropogenic sources strongly affect atmospheric composition and impact on climate, air quality and, indirectly, on the evolution of the cryosphere. Quantifying emissions is one of the major challenges for the development of air quality and climate policies (Fowler et al., 2009; Isaksen et al., 2009) and this should account for differences in the temporal changes of human-related emissions and natural emis-

TCD
7, 6001–6042, 2013

sions as well as in their geographical distribution. Large uncertainties in past and current global inventories of anthropogenic and natural emissions limit the establishment of a reliable framework of emission inventories required for realistic emission scenarios. This is especially true for the Indian subcontinent for which reliable estimates of past and current emissions are crucially lacking. India is one of the two largest anthropogenic aerosol generating countries in the world (Lu et al., 2011). In the past decade, India has been identified as a hot spot in terms of high aerosol optical depth (AOD) observed from space (Prasad and Singh, 2007) with components such as sulfate, organic carbon (OC) or black carbon (BC) playing a very active role. India on its own contributes 10 to 20 % of all current emissions globally (Bond et al., 2007) and has therefore received the greatest attention from compilers of emission inventories.

Recent works performed within the "Atmospheric Brown Cloud" and the "SHARE" projects (http://www.evk2cnr.org) indicated that the south-facing side of the Himalayas is particularly affected by emissions from the Indo-Gangetic plains. Unique atmospheric observations team at the global GAW (Global Atmosphere Watch) station of Nepal Climate Observatory-Pyramid (NCO-P) located at 5079 m a.s.l. on the southern foothills of Mt. Everest (Bonasoni et al., 2010), documented for the first time the efficient transport of short-lived climate pollutants (SLCPs) to the high altitude. Continuous observations over more than 7 yr revealed very high concentrations of SLCPs in particular BC (Marinoni et al., 2010) and ozone (Cristofanelli et al., 2010) especially in pre-monsoon season. The presence of light absorbing material affects the radiative balance of the atmosphere both at local (Marcq et al., 2010) and at a regional scale. Source areas of aerosols have been clearly identified for the high Himalaya by (Cristofanelli et al., 2010) and are located in the Indo-Gangetic plains for most part of the year. Source origin for aerosol species is likely linked to biofuel combustion (Decesari et al., 2010). Desert dust events are also regularly observed at NCO-P, either mixed with anthropogenic pollution from Pakistan and/or directly from Gobi desert (Bonasoni et al., 2010). Black carbon and dust are efficiently scavenged to the snow/ice surface by dry and wet deposition (Yasunari et al., 2010, 2013); these impurities can lead to surface albedo re-

TCD
7, 6001–6042, 2013

duction, especially in visible wavelengths, that increases heating, accelerating ice and snow melting.

Ice cores contain information about past temperatures, precipitation and past deposits of many important species, both short-lived (reactive gases, particulate matter and semi-volatile species) and long-lived (CO_2 and other greenhouse gases). They have been used in the past for providing independent records of past aerosol load and composition, as for example by (Preunkert and Legrand, 2013) for Europe. For the Himalayas, most studies were performed over the Tibetean plateau (i.e. Thompson et al., 1989, 1990, 2000) where the impact of Indo-Gangetic plains emission is reduced because of dominant westerlies circulation. The southern margin of the Himalayan range is influenced by the seasonal alternation of the westerlies and the Indian monsoon: the study of ice cores extracted on Mount Everest – East Rongbuk glacier (28° N, 87° E) made profit of this alternance even if this glacier is situated in the northern flank of the Himalaya range. The East Rongbuk site provided a spectrum of climatic and environmental records including chemistry and isotopes (Kang et al., 2002; Kaspari et al., 2009; Zhang et al., 2009; Lee et al., 2011), dust (Xu et al., 2010) as well as the first profile of BC (Ming et al., 2008; Kaspari et al., 2011). The southern flank of Himalaya, where Mera Glacier drilling site is located, is more influenced by monsoon and by southern pollution events than the Rongbuk site.

Radiative forcing of BC in snow and associated enhanced melting have raised attention of the scientific community in recent years. Several experimental and modeling studies came to the conclusion that impact is measurable in the Himalayan regions (Flanner et al., 2012; Sterle et al., 2013; Ming et al., 2009). For example, the atmospheric concentration of BC at NCO-P station was converted into albedo change potential by (Yasunari et al., 2010) concluding that BC deposition may increase the glacier water runoff of about 70–204 mm annually. However, the effective impact of increased BC deposition flux in term of glacier melting is still very uncertain. While some studies using snow/ice cover simulation from aerosol emission inventories have attributed the decline of simulated Himalayan snow/ice cover for the 1990–2000 period to enhanced

TCD
7, 6001–6042, 2013

Indian BC emissions (Menon et al., 2010), the recent study of Bond et al. (2013) pointed out the very large uncertainties associated with such studies.

Part of this uncertainty is linked to the strong deficiency in observations for the Himalayan region, from glacier mass balance to atmospheric composition data at high altitude, over 6000 m a.s.l., where glaciers are snow covered all around the year. In order to focus our study to a site mainly influenced by the Indian monsoon, our action was directed onto the southern slope of the Himalayas. Here, we present the first results from an ice core extracted from Mera Glacier (6376 m a.s.l., 27°43′ N, 86°52′ E) in Nepal. We investigate, together with radiation modeling, the impact of refractory black carbon (rBC) and dust on seasonal surface albedo changes and induced potential melting over the last decade.

2 Site description and experimental methods

2.1 Local climatology

The site is located about 30 km South of NCO-P, a GAW global station providing since March 2006 continuous observations on meteorological parameters and atmospheric composition. Meteorological characteristics and air mass circulation affecting NCO-P and Mera Glacier drilling site are well described in (Bonasoni et al., 2010) and in agreement with the local weather regime, we define the seasons as pre-monsoon from March to May, monsoon from June to September, post-monsoon from October to November and Winter from November to January. Large-scale Asian monsoon circulation and local mountain wind system control the atmospheric conditions in the Himalayan high-altitude valleys. 80 % of the annual precipitations are concentrated between June and September (Wagnon et al., 2013; Bonasoni et al., 2010) and influenced by the summer monsoon (Bonasoni et al., 2010; Ueno et al., 2008; Bookhagen and Burbank, 2006). Large scale circulation affecting the Himalayan southern slopes can be described as a balance between eastward traveling disturbances during cold season (October to

TCD
7, 6001–6042, 2013

May), and monsoon depressions from the northern Gulf of Bengal during the rest of the year. The synoptic origins of the air masses reaching this region are related to these circulation patterns. During monsoon, 96 % of the air masses are regional or originate from the Gulf of Bengal, while during winter (December–March) and post-monsoon (October–November), westerlies circulation favors the transport from north-east West India, Pakistan and the Middle East. During pre-monsoon (April–May), high aerosol concentration is reported by atmospheric observations and related to the direct transport of brown cloud pollutants to the Himalayas (Hindman and Upadhyay, 2002; Bonasoni et al., 2010). The concentration of particles in the atmosphere measured at NCO-P shows two maxima, during pre- and post-monsoon seasons, while the minima during monsoon correspond to the efficient washout of particles by rain before reaching the Himalayas (Sellegri et al., 2010).

2.2 Field campaign

In the southern slope of the Himalayas, only a few glaciers are suitable for ice core investigations with the expected characteristics in terms of temperature, geometry, accumulation rates, access and safety. A site was identified in the accumulation zone of Mera Glacier (6376 m a.s.l., 27°43′ N, 86°52′ E) in Nepal, on the Himalayan south range, a glacier studied since 2007 within the framework of SOERE Glacio-Clim/Himalaya for mass/energy balance (Fig. 1). The site has a mean annual temperature below −5 °C. The selection was also based on the monsoon trajectories and natural and anthropogenic compounds source areas, in order to provide reliable records for the monsoon record study.

The 19.8 m long firn core was extracted using an electromechanical FELICS small drill (Ginot et al., 2002) on 11 November 2010. Core density and stratigraphic markers were measured during drilling. The core was immediately logged and sub sampled in the field. 276 samples, of an average length of 6.6 cm (between 4 and 16 cm) were stored into 276 sealed pre-cleaned polypropylene vials and kept in insulated core box for transport. Since the cold chain could not be assured from the glacier to the

TCD
7, 6001–6042, 2013

laboratory and that the samples were going to melt during shipment, a few drops of formaldehyde solution were added to the samples in order to limit the bacteriological development in the vials. Temperature logger in the box recorded that samples were melted during 18 days of shipment before being refrozen in the laboratory.

2.3 Sample analyzes

Analyzes of major and organic chemical species were performed using a Dionex© ICS3000 dual ion chromatography system at LGGE. The chromatography system was setup for the analyzes of cations (Li^+, Na^+, NH_4^+, K^+, Mg^{2+}, Mn^{2+}, Ca^{2+} Sr^{2+}) and anions (F^-, Cl^-, NO_2^-, Br^-, NO_3^-, $(CH_2)_2C_2O_4^{2-}$, SO_4^{2-}, $C_2O_4^{2-}$) down to sub-ppb level and high level accuracy (6 standards calibration, relative standard deviation < 2 %). Other species determination was disturbed by the formaldehyde spiking. Insoluble dust measurements were performed using a microparticle counter (Coulter Counter© Multisizer III) for particles with equivalent diameter from 1.0 to 30 µm, divided in 300 equivalent size channels. The total mass of dust has been calculated from the volume size distribution assuming a density of 2.5 g cm^{-3}. Analytical systems are set up in the class-100 clean room of LGGE laboratory. Detailed analytical procedure and accuracy are described in (Delmonte et al., 2002).

The ^{18}O content of the ice was measured at the LAMA laboratory of HydroSciences Montpellier, on an Elementar Isoprime Mass Spectrometer coupled with an Aquaprep module, using the classical CO_2 equilibration technique. The results are expressed in $\delta^{18}O$ on the V-SMOW scale with an overall uncertainty of ±0.06‰. Half of the samples that were analyzed for chemical composition were measured for $\delta^{18}O$, which corresponds to a resolution of approximately 12 cm of snow.

The SP2 uses a laser-induced incandescence technique to measure the mass of individual refractory BC (rBC) independently from rBC particle morphology and light-scattering coating materials (Petzold et al., 2013; Cross et al., 2010; Moteki and Kondo, 2007, 2010; Schwarz et al., 2006). A single rBC particle passing through the laser

TCD
7, 6001–6042, 2013

beam intra-cavity absorbs light, reaches a vaporization temperature at which it incandesces, and emits visible thermal radiation. The incandescence signal is proportional to the mass of the individual rBC particle. Fullerene soot was used for calibration of incandescence signal. Use of SP2 for liquid samples requires nebulization which was performed by an APEX-Q, (EPOND, Switzerland) system. The efficiency of the APEX/SP2 system is accounted for applying a correction factor of 0.56 to rBC mass concentration in all samples. For rBC particles, we used the sum of individual rBC particle mass from ~ 50 to 600 nm mass equivalent diameter to obtain rBC mass concentration of each sample. Over the whole record, the highest number of particles appears between ~ 50 and 90 nm mass equivalent diameter (Lim et al., 2013).

The measurement of equivalent BC in the atmosphere, resulting from the aerosol absorption coefficient measure, was obtained at NCO-P by MAAP (Multi-Angle Absorption Photometer, © Thermo): it measures the transmission and the back scattering of a light beam (Petzold and Schönlinner, 2004) incident on a fibre filter where aerosol particles are deposited by sampling flow. The detection limit (3σ of blank measurements) was calculated as 11 ng m^{-3}, with an integration time of a 30 min basis (Marinoni et al., 2010).

3 Ice core records

3.1 Dating

The firn core was annually dated between 2010 and 1999 based on seasonal cycles of stable isotopes and chemical proxies. In this region, the stable isotope composition of precipitation is mostly controlled by the rainout effect associated to the Indian monsoon activity (Araguás-Araguás et al., 1998; Zhang et al., 2001; Vuille et al., 2005). Precipitation data collected during one year at the high altitude GNIP Lhajung station (27°53′42″ N; 86°49′30″ E; 4420 m a.s.l., Nepal) (International Atomic Energy Agency/World Meteorological Organization, 2006), showed depleted values

TCD
7, 6001–6042, 2013

(min δ^2H = −130.4‰) related to the monsoon rain season (June), while enriched values (max δ^2H = −18.9‰) corresponding to pre-monsoon season (March–May), resulting in a seasonal amplitude of 111.5‰ for δ^2H (≈ 13.9‰ for δ^{18}O considering the slope of the Global Meteoric Water Line). The clear δ^{18}O variation recorded along the core, about 10‰ in amplitude (Fig. 2) can safely be related to seasonal cycles, with the depleted phase corresponding to monsoon season and enriched peaks to post-monsoon/winter/pre-monsoon. Since precipitation is reduced during non-monsoon seasons at high altitude, part of the enriched events may be missing from the record due to eventual snow wind erosion (Wagnon et al., 2013) resulting in a reduced seasonal amplitude compared to drainwater values.

Variation of chemical tracers in the ice core is used to complement the stable isotope records for dating purposes. In order to observe the highest seasonal variability in the chemical composition, we focused on species subjected to a combination of deposition processes like scavenging and post-deposition enrichment (Ginot et al., 2001). The difference between wet monsoon and dry winter and their related aerosol sources and deposition processes is amplified with this approach. Ammonium ion (NH_4^+) is for these reasons a good indicator. The potential sources of ammonia in this region are biomass burning, farming and soil emission resulting from the use of nitrogen fertilizers (Sun et al., 1998). As observed in the atmospheric record at NCO-P (Decesari et al., 2010), similarly to the main aerosol chemical constituents, NH_4^+ undergoes strong seasonal variability with minima during the monsoon periods and maxima during the pre-monsoon. During monsoon season, NH_4^+ is efficiently washed out by precipitation and does not reach the high Himalaya leading to annual minima (Decesari et al., 2010; Carrico et al., 2003). During post-monsoon and winter corresponding to drier conditions, a rise of NH_4^+ concentration is observed in the atmosphere and a clear strong peak is then usually recorded during pre-monsoon season. Dry and wet deposition processes for both particulate NH_4^+ and gaseous NH_3 produce high concentration peaks on the surface snow, that may subsequently be amplified by post-depositional processes such as snow sublimation (Ginot et al., 2001) or reaction with HNO_3 absorbed on the snow

TCD
7, 6001–6042, 2013

layers (Marinoni et al., 2001; Shrestha et al., 2002). During winter, westerly circulation associated to distant or reduced sources may generate low NH_4^+ concentration in the snow layers; but these layers are usually scarce (very dry conditions in winter) and often not preserved in the snow column (snow remobilized into the atmosphere due to strong winds at high elevations in winter, Wagnon et al., 2013). The ammonium core profile was therefore used for dating, with high concentration peaks corresponding to the annual dry season (Fig. 2).

Isotopic and chemical dating methods result in a seasonally resolved dated profile ranging from November 2010 to 1999 (Fig. 2). The lowest NH_4^+ concentration layer observed between the surface and 1.19 m water equivalent (w.e.) depth, also corresponding to the most depleted $\delta^{18}O$ over the whole profile, is atypical in the profile and was related to the temporary preservation of pre-early winter snow from September to November 2010. This layer was composed by cold small loose snow grain, in opposition to the deeper part of the core composed by more compact, larger and transformed snow crystals and ice layers. Such early-winter snow layer is not preserved elsewhere along the profile probably because of strong wind erosion and loose snow remobilization during winter as systematically observed on-site by Wagnon et al. (2013) since 2007.

The profile was divided into three seasonal patterns. As said earlier only one single winter event was identified between surface and 1.19 m w.e. depth. The snow fraction related to monsoon and inter-monsoon conditions was attributed according to the $\delta^{18}O$ composition. Along the profile, 68 % of the core is attributed to "monsoon", 24 % to "inter-monsoon" and 8 % to "winter" layers.

3.2 Observed concentration profiles, deposition processes and seasonal fluxes

The ice core record is characterized by a strong seasonality that can be sub-divided into 3 distinct patterns corresponding to winter, monsoon and inter-monsoon. Table 1 summarizes concentrations of major ions, dust and rBC for the whole core and for

TCD
7, 6001–6042, 2013

the 3 distinct periods. The column "winter" is derived only from the available layer of September–November 2010.

Whereas major ions concentrations (NH_4^+, NO_3^-, SO_4^{2+}, Ca^{2+}, F^-) are in the same order of magnitude as observed by (Ming et al., 2007) on the northern side of the Himalaya, at the East Rongbuk Glacier, the aerosol sources or deposition processes, characterized with species ratios, are different as elsewhere. In our study, Ca^{2+} represents the major ion, in accord to the high dust concentration observed in the atmosphere at NCO-P (Decesari et al., 2010). The mean concentration ratio $[Ca^{2+}]/[SO_4^{2-}]$ is equal to 4.33, but only 0.23 from aerosol/snow study at East Rongbuk Glacier site on the Northern Himalayan slope (Ming et al., 2007). According to the ionic balance (ΣCations – ΣAnions) mostly negative and the high $[Ca^{2+}]/[SO_4^{2-}]$ ratio, calcium seems to be mostly associated as calcium carbonate ($CaCO_3$) whether as gypsum ($CaSO_4$).

Black carbon averaged level in the ice core is $3\,\mu g\,L^{-1}$, with maxima during inter-monsoon seasons ($9.25 \pm 9.69\,\mu g\,L^{-1}$) and minima in monsoon season ($1.06 \pm 1.52\,\mu g\,L^{-1}$). These values can be compared with previous studies on ice core in Tibetan Plateau, such as (Ming et al., 2008) and (Kaspari et al., 2011), accounting for the fact that different techniques are used that are not directly comparable (Petzold et al., 2013). Concentrations measured at Repula Col by (Ming et al., 2008) using the thermal-optical methods for present conditions are higher ($20.3 \pm 9.2\,\mu g\,L^{-1}$) but lower for East Rongbuk glacier analyzed with SP2 method (Kaspari et al., 2011) with only $0.7 \pm 1.0\,\mu g\,L^{-1}$.

Insoluble dust shows a high mean concentration level ($10.1\,mg\,L^{-1}$), with only few spikes up to $66.9\,mg\,L^{-1}$ before monsoon layer of 2003. This mean value is much higher than the $0.465\,mg\,L^{-1}$ mean value measured on the opposite slope of Mount Everest, central Himalaya, ice core (Xu et al., 2010). The relative lack of seasonality in the dust record is surprising and may reflect the fact that a high background level of dust input, whether from a local source or a regional source, is impacting on the dust record. Figure 3 shows the mean size distribution of dust for the 3 periods of interest. Presence of large particles > 10 µm is confirmed at all time and the modal size distri-

TCD
7, 6001–6042, 2013

bution of dust is quite similar between winter, monsoon and inter-monsoon seasons, with respectively a mean mass equivalent diameter of 5.7 µm, 6.0 µm and 6.4 µm respectively. The mean dust concentration shows some seasonal differences with lower value in winter (7.2 mg L^{-1}) and higher concentration during monsoon (10.1 mg L^{-1}) and inter-monsoon (11.1 mg L^{-1}). This is similar to observations of (Gobbi et al., 2010) using sunphotometer signal but contradicts observations made at NCO-P by (Marinoni et al., 2010). The layer with the highest concentration of dust recorded at 8.9 m w.e. depth with 66.9 ppm (Fig. 1) shows a larger mean mass equivalent diameter of 10 µm. This event could by associated to a major dust outbreak over south Asia in June 2003, described by (Gautam et al., 2013). The process by which dust is deposited to snow at Mera is uncertain but concentrations are clearly higher than expected by atmospheric measurements at NCO-P.

Empirical Orthogonal Factorization (EOF) can be used for analyzing the behavior of the different species. The variance analysis was first performed on the totality of samples. Not surprisingly, most of the variability (Principal Component 1 – PC1 = 34 %, all species) is mainly controlled by the deposition processes themselves that fore used for dating purposes. All ions concentrations correlate with low (high) concentration during wet- (dry-) season. $\delta^{18}O$ and soluble ionic species are in phase, with depleted (enriched) isotopic values with low (high) concentrations. The seasonal variation of dust does not appear clearly in Fig. 2 and association of PC1 is driven by sporadic peaks during the inter-monsoon. The second PC2 and third PC3 factors explain limited variance (15 % and 11 % respectively) and can be used to differentiate behavior of salts such as Cl^-, Na^+, K^+ and Li^+ on one side, possibly linked to emissions from salt lakes located in the Tibet area and with terrigeneous material such as Ca^{2+} on the other side from the behavior of all other species.

Observed maxima during the inter-monsoon period is connected to dry deposition process that accumulates the impurities on the snow surface, amplified by snow sublimation (Ginot et al., 2001). This effect seems particularly important for rBC and fluoride deposition that reveals thin high concentration inter-monsoon peaks along the record,

TCD
7, 6001–6042, 2013

up to 47.90 $\mu g L^{-1}$ for rBC. Moreover, the analysis of transport of both dust and pollution, as observed from NCO-P station, indicates the periods of maximum transport of pollution and dust in non-monsoon seasons.

As observed in Fig. 2, no obvious trend can be detected from the overall 10 yr ice core record for any of the species of interest. Using the ECCAD portal (http://eccad.sedoo.fr) and the MACCity inventories (Granier et al., 2011; Lamarque et al., 2010; Diehl et al., 2012; van der Werf et al., 2006), we calculated the temporal variability of anthropogenic and natural emissions for the area of Northern India/Pakistan most influencing the high Himalayan regions (selected area: India+). During the 1999–2010 period, it is estimated that anthropogenic emissions of SO_2, NO_x and BC have increased by 56 %, 45 % and 20 %, respectively. No trends are observed for anthropogenic NH_3 emissions, or for biomass burning emissions of any of the 4 species. As seen in Fig. 2, no trend is detected in the ice core record over the last 10 yr for any of the considered species. Emission intensity is peaking during the winter period which is not associated with the highest concentrations in the ice core record as the winter snow layers are not preserved. Development of thermal breeze or weak convective process limits efficient transport from the Indo-Gangetic plains to the higher altitudes during that period. When compared in terms of fluxes, over this 10 yr time span, the variability in the ice core signal is rather reflecting the variability of the monsoon signal than that of emission intensity in the India+ area. This is an important result for studies connecting BC emissions to their impact on the cryosphere.

3.3 Comparison with the aerosol record at NCO-P

The atmospheric composition has been continuously measured at NCO-P since March 2006 (Fig. 4). We therefore can compare the atmospheric observations recorded at NCO-P with the signal of Mera ice core during the overlapping period from 2006 to 2010. NCO-P and Mera Glacier are distant of approximately 30 km and 1300 m in elevation. Because intensity in the ice core signal is a complex result of wet scavenging,

TCD
7, 6001–6042, 2013

dry deposition and post-depositional processes, it is difficult to directly relate to an atmospheric signal. In addition, techniques used to reconstruct the ice core signal differ generally from those used in the atmosphere and cannot be easily compared. PM_{10} filters are regularly sampled at NCO-P and analyzed. Elemental and organic carbon as well as major ion concentrations are measured at NCO-P. Black carbon is measured by single-particle incandescence, correlated to black carbon mass, in the snow and derived from aerosol absorption coefficient in the atmosphere. Very few comparisons between these two techniques are available. Dust is measured in the snow by Coulter Counter and approximated by PM_{10}-PM_1 signal of the optical particle counter (OPC) in the atmosphere. Similarly, without additional information on shape, density and refractive index, the 2 records cannot be compared quantitatively. However, similarities and differences can be pointed out.

Comparisons between the ice core signal at Mera Glacier and the atmospheric observations at NCO-P are shown in Fig. 4 for BC and dust. In order to reconstruct both signals along the same temporal axis, we use the continuous observations carried out at NCO-P, and for the firn core, we have converted the depth scale to time using the following procedure. The seasonally resolved record allows reconstructing the evolution of snow surface concentration for rBC and dust. For monsoon season, set between 1 June and 30 September, we approximate the concentration as a constant calculated from each year "monsoon" season mean, and for following inter-monsoon season, we started at monsoon level and increases linearly until maximum "inter-monsoon" season value (Fig. 4).

Both atmospheric and ice core records show strong seasonality with the smallest values observed during the monsoon season and highest values during the inter-monsoon (or pre-monsoon). The conjunction of emission, transport and deposition (wet or dry) favors presence of short-lived species (and BC in particular) in snow during the February/June period. The variability of the dust signal is much less pronounced in the ice core signal with respect to the atmospheric signal, as seen from Figs. 3 and 4. The ratio between mass of dust and rBC in the ice core signal is much higher than that of

TCD
7, 6001–6042, 2013

(PM_{10}-PM_1) and equivalent BC in the atmosphere. This is an additional confirmation of the presence of a local dust source, formed with coarse particles not sampled in the PM_{10} inlet at NCO-P.

The snow is clearly enriched in NO_3^- and NH_4^+ with respect to the atmosphere, if we take SO_4^{2-} as a reference. While NO_3^-/SO_4^{2-} and NH_4^+/SO_4^{2-} rarely exceed 1 (average = 0.42 and 0.50 respectively) in the atmosphere (Decesari et al., 2010), they are much higher in the ice samples (average = 1.32 and 2.89, respectively). This is certainly due, on one side, to negative artifact on the filters leading to loss of NO_3^- (and NH_4^+ to a lesser extent) but also to efficient scavenging (wet and dry) of highly soluble NH_3 and HNO_3 gases to snow surfaces.

3.4 Dust and rBC deposition fluxes

Annual deposition fluxes can be compared at both sites, with a few assumptions for the overlapping period 2006–2010. Here we have limited the calculation to BC from atmospheric measurements using deposition velocities derived by Yasunari et al. (2010, 2013). For the pre-monsoon season 2006, Yasunari et al. (2010) have obtained a total BC deposition amount of 0.266 mg m^{-2} at NCO-P. The time evolution of the surface snow concentration is simulated using the firn core data and the dating procedure described previously and illustrated in Fig. 4. This reconstruction is used to simulate the impact of surface snow impurities impact on glacier energy balance and melting (Sect. 4.3).

Deposition fluxes for some specific aerosol like rBC and insoluble dust were calculated from the ice core data. Annual mean deposition fluxes (from 1 October to 30 September) over the last 10 yr are 3.2 ± 1.2 mg m^{-2} yr^{-1} for rBC and 10.1 ± 2.5 g m^{-2} yr^{-1} for dust. This value for rBC is in the upper range of fluxes modeled by (Yasunari et al., 2013) for this region of the Himalaya, and one order of magnitude higher that calculated from NCO-P station pre-monsoon measurements (Yasunari et al., 2010). Furthermore, these fluxes were calculated between monsoon and

TCD
7, 6001–6042, 2013

inter-monsoon regimes. If we apply the seasonal fluxes splitting between "monsoon" and "inter-monsoon", we can observe that rBC and dust presents different behaviors. Dust mean concentration is still higher during inter-monsoon season (66.9 mg L^{-1}, vs. 26.5 mg L^{-1} during monsoon) but the deposition flux during monsoon represents 72 % of the annual flux. On the opposite, the rBC deposition flux is concentrated during inter-monsoon, with 75 % of the annual deposition, and with a higher mean concentration contrast between season (9.25 µg L^{-1} during inter-monsoon, 1.06 µg L^{-1} during monsoon).

As dust shows high deposition fluxes for all seasons, we used the available data to track source changes. Soluble species analyzed by ion chromatography as calcium, magnesium, manganese and strontium were used to calculate ratios of soluble ionic species vs. dust. The negative ionic balance is attributed to the carbonate load. These ratios and carbonate are used to identify some changes in the dust sources. The ionic balance is negative all over the record (−6.7 µEq L^{-1} mean value), but with a weak higher value for winter snow (−4.5 µEq L^{-1}) and some spikes ranging down to −20 to −40 µEq L^{-1}. The calcium/dust ratio is quite stable over the record. The two dustiest layers located during inter-monsoon, at 4.1 and 8.9 m w.e. depth are atypical (Fig. 2), with highest carbonate concentration and high ratios of manganese and magnesium, which may characterize a different dust source that was not identified. A third source, with high lithium ratio associated with sea salt, and with or without carbonate is reported in the most recent part of the record (winter and monsoon 2010), and could represent inputs of aerosols coming from salt flat or saline lakes located in the Tibetan plateau.

As we can see in Fig. 2, rBC concentration peaks build up between each annual monsoon event, during the drier period. According to the observation at NCO-P station (Marinoni et al., 2010), the highest atmospheric BC concentration occurs during pre-monsoon season (February–May) and is transported both by valley breeze form Indo-Gangetic Plain (India, Nepal) and by longer range from Middle East and Europe sources air masses. The deposition occurrence between BC and other anthropogenic

TCD
7, 6001–6042, 2013

activities tracers, like ammonium and fluoride, confirm the regional source associated to the "brown cloud".

4 Dust and rBC impact on surface albedo and glacier melting

4.1 Albedo changes with BC and dust deposition

For this study, we used the ice core based aerosol fluxes reconstruction to investigate the impact of dust and rBC contents of the snow surface on its energy balance by changing the surface albedo. Our approach was to simulate the resulting albedo change produced by different impurity concentrations, dust and rBC, measured from the ice core. For this purpose, we used the radiative transfer model DISORT (Stamnes et al., 1988) with several simplistic assumptions since we aim at providing order of magnitude of the impurity effects on the snow radiative balance.

The snow grains are considered as spherical and we used Mie theory to compute their single scattering properties. The refractive index of ice is taken from (Warren and Brandt, 2008). The refractive index of BC and its density is taken from (Flanner et al., 2012) whereas the refractive indices and density of dust with different contents of hematite are taken from (Balkanski et al., 2007). DISORT model was used to simulated the spectral albedo of an external or internal mixture of impurities and snow as detailed in (Flanner et al., 2012). In the absence of any measurement, the snow grain size was chosen as constant over the profile (optical radius (r_opt) of 0.16 mm or 0.65 mm) and the impurities were equally distributed into the snowpack (internal or external).

Dust and BC contents were computed from the seasonally dated core record. Dust is considered as being external to the snow grains given its size (mass equivalent diameter ranging from 6 µm when deposited with precipitation up to 10 µm when transported dry). BC is assumed as being external during the dry season (dry deposition) and internal during the monsoon (wet deposition). BC mean diameter is taken as 90 nm for all seasons as shown by SP2 the measurements.

TCD
7, 6001–6042, 2013

The simulated spectral albedo using DISORT for the 1 June 2003 and the 1 June 2005 and for diffuse irradiance is illustrated for examples in Fig. 5. These two dates were chosen as they represent extreme values of dust and rBC content in the record at the end of the simulated post-monsoon season. For June 2003, the rBC content is 26.64 ppb and the dust content is 66.9 ppm whereas for June 2005, the rBC content is 47.9 ppb and the dust content is 13.13 ppm. The blue solid line corresponds to the albedo of pure fine snow (r_opt = 0.16 mm) while the black solid line is the albedo of fine snow containing both rBC and dust. The two red lines correspond to the spectral albedo of pure and contaminated snow for coarser grains (r_opt=0.65 mm). For these simulations we choose a hematite content of 1.5 % for the dust refraction index which corresponds to the average content determined by (Balkanski et al., 2007). In the 350–500 nm range for fine grains, impurities caused a decrease of about 0.1 of the value of the albedo for June 2003 whereas only dust implies a decrease of 0.05 for June 2005 (around 0.1 for 2003) and only rBC implies a decrease of around 0.05 for the two years. This figure enhances the fact that the impurities have a non linear effect on the value of the albedo. Indeed rBC and dust combined together have less effect than the sum of the effects of only rBC and only dust. This can be easily explained by the fact that a mixture of impurities and snow has a much higher absorption coefficient (imaginary part of the refractive index) than pure snow. Thus adding one type of impurity to the snow diminishes the impact of the other impurity compared to the impact of the same amount of impurity on pure snow. In other words, the higher the absorption coefficient is, the less the impact of supplementary impurities will be. The effect of snow grain size is also noticeable on this figure while comparing the simulations. The same amount of impurities has more effect on coarse grain snow than on fine grain snow. Indeed, the albedo decrease due to impurity in the visible range is at least two times higher for coarse grains than for small grains since photons generally travel a greater distance in the snow pack for coarser grains (Warren and Wiscombe, 1980). Different content of hematite were tested, minimal (0.9 %) and maximal (2.7 %) according to (Balkanski et al., 2007), and illustrated in Fig. 5. It shows the impact on the albedo of the refractive

TCD
7, 6001–6042, 2013

index of dust chosen in the simulation. In the following, we will only use the average value of 1.5 % for the hematite content.

4.2 Additional absorbed energy

To evaluate the amount of additional solar energy absorbed by the snowpack due to the presence of impurities, it was necessary to estimate a mean solar incident radiation incident and its characteristics. The solar irradiance was therefore computed using the radiative transfer model SBDART (Ricchiazzi et al., 1998). SBDART is based on the same computation rules than DISORT. It considers an atmosphere made of different plane parallel layers. The characteristic of the atmospheric profiles (aerosols, water vapor, ozone ...) are set according to the site location. The solar zenith angle was selected according to the location and the hour of the day. The sky is assumed to be clear for all days in the clear sky simulation and cloudy for alldays in the cloudy simulation. One simulation was done at the beginning of each month during the 11 yr of the study. For each day, the diurnal cycle of the energy absorbed by the snowpack was reconstructed, and interpolated on a daily basis over the whole period.

Figure 6 presents for the year 2003 the daily mean surface forcing due to impurities. These daily values correspond to the difference between the solar energy absorbed by a pure snowpack and the energy absorbed by a contaminated snowpack. The simulation shows that the radiative forcing of impurity is maximal for the pre-monsoon season, up to 40 $W m^{-2}$ for clear sky and coarse grains snow, as also observed by MODIS investigation (Gautam et al., 2013). For 2003, 75 % of the radiative forcing can be attributed to the presence of dust in the snowpack. The Fig. 6 shows also that the radiative forcing is twice greater for coarse snow (r_opt=0.65 mm) than for fine thin snow (r_opt=0.16 mm). These results are comparable with those provided by (Sterle et al., 2013) in the Sierra Nevada snow. Moreover cloudy sky induces half radiative forcing compared to clear sky simulation (maximum radiative forcing of 24 $W m^{-2}$ for coarse snow grains).

TCD
7, 6001–6042, 2013

The whole period covered by the ice core, 2000–2010 was finally simulated (Fig. 7). It appears clearly that the high dust content is mainly responsible of most for the additional absorbed energy. The effect of rBC is indeed, except for some high rBC concentration peaks (e.g. June 2006), much lower that the dust effect. Over the whole period, the total impurities are responsible for a 6.3 % increase of the absorbed energy in case of fine snow, with 5.3 % related to dust and 1.3 % to BC compared to pure snow. In case of coarse snow consideration, the impact is more important reaching 12 % increase of absorbed energy.

4.3 Potential melting evaluation

The impurities deposited on the glacier surface increase the absorbed energy and have an impact on the glacier melting. Here we only estimate a potential excess melt rate attributed to impurities over years for each season (dry or monsoon) over the experiment period. The melt rate has been calculated using the mean value for clear sky and cloudy sky simulations and for the average of coarse snow and fine snow radiative forcing. In order to represent the melt caused by the impurities any given day the following assumptions have to be done, (a) all other terms of the surface energy budget corresponding to turbulent fluxes and long wave net radiation, were remained unchanged and, (b) the snowpack was at the fusion temperature. The resulting values are illustrated in Fig. 8. It is important at this point to noteworthy that almost no melt occurs in the highest part of the glacier and at the location of the ice core drilling, because the firn temperature always remains below the melting point except for some exceptional events, as confirmed by the core analyzes that show only sign of very limited refreezing layers. Nevertheless, this study can help evaluating the additional melt due to the presence of the same quantity of impurities in the lower part of the glacier where melt does occur in summer assuming that dust and BC contents are equally distributed over the glacier. This later assumption needs to be further investigated since e.g. in the ablation area of the glacier, the melt water might “wash” the snow surface by dragging the impurities, or impurities could concentrate on ablation surface (Sterle et al., 2013).

TCD
7, 6001–6042, 2013

If it is well demonstrated that the impact of dust is much higher that BC on the potential melt for Mera Glacier, it is interesting to observe that this impact does not change much over seasons, with moderately higher values during the dry season (with higher impurity content) than during the monsoon season (Fig. 8). This is mainly related to lower solar irradiance during part of the dry season (winter) compared to the summer irradiance. These results might thus vary while considering the effect of clouds during the monsoon only and according to localization on the glacier depending on the aspect and shading.

4.4 Comparison with glacier energy and mass balance

Dust and rBC particles snow content increases the glacier surface melting in some areas of the glacier. Their impact, as illustrated in Fig. 8, is estimated at an annual mean melting of $+1.8\,kg\,m^{-2}\,d^{-1}$ for dust and rBC, with the fraction related to rBC only of $+0.78\,kg\,m^{-2}\,d^{-1}$ and $+0.19\,kg\,m^{-2}\,d^{-1}$ during inter-monsoon and monsoon respectively. These rates correspond to about $+662\,kg\,m^{-2}$ annual melting associated with dust and rBC, and $+214\,kg\,m^{-2}$ for rBC only.

In order to evaluate this impact on Mera glacier, we compare these values with mass-balance and energy-balance measurements taken on the glacier since 2007. The melting rate is calculated from the energy balance using as input data measurements from the free standing automatic weather station (AWS) located in the ablation zone at the elevation of 5360 m a.s.l. The specific mass balance is calculated annually from a stakes network and topographical data derived from Pleiade satellite image of 2012 (Wagnon et al., 2013). For the year 2009–2010 at 5400 m a.s.l., the mass balance measurement gives an annual point-mass balance of $-2280\,kg\,m^{-2}\,yr^{-1}$ (corresponding to annual snow accumulation minus annual ablation), whereas energy balance approach results in an annual melting of $4300\,kg\,m^{-2}\,yr^{-1}$ melting without taking into account sub-layers refreezing. Considering that in 2009–2010, the net accumulation measured at the highest part (6330 m a.s.l.) of Mera Glacier is $720\,kg\,m^{-2}$ (Wagnon et al., 2013), annual accumulation at 5400 m a.s.l. is at least $720\,kg\,m^{-2}$ making the

TCD
7, 6001–6042, 2013

effective melting at 5400 m a.s.l. higher than 3000 kg m^{-2} (= 2280 + 720). The correct melting value is in turn comprised between these previous 3000 and 4300 kg m^{-2}. The melting related to impurities calculated in this study for the year 2009–2010 correspond to +543 kg m^{-2} yr^{-1} annual melting associated to dust and rBC, and +215 kg m^{-2} yr^{-1} for rBC only.

If we compare these values, it appears clearly that, with all our assumptions and considering a site where firn is close to 0 °C, total impurities control a maximum of about 18 % of the melting, when rBC alone accounts for a maximum of about 7 % only at 5400 m a.s.l. Some intuitive consideration for a spatial distribution over the whole glacier would conclude to much less impact for the impurities on glacier melting. Mera Glacier specific mass balance measured between 2007 and 2012 results in −100 ± 400 kg m^{-2} yr^{-1} (Wagnon et al., 2013). The impact of rBC on the mass balance is estimated to be lower than its inter-annual variability, while the impact of dust and BC together can be of the same order of magnitude.

4.5 Limits of the simulations

The simulations presented in this section rely on a range of simplistic assumptions. These assumptions have been used to circumvent some difficulties: the exact profile of impurity content in the snowpack was not translated into surface concentration evolution, meteorological conditions (clouds, precipitations . . .) were not taken into account and surface conditions over the whole glacier area have not been taken into account either. Snow metamorphism was not taken into account either and in the simulation ice grains are supposed to be spherical (Libois et al., 2013). Nevertheless, the results presented here are deduced from the difference between the solar radiation budget for pure snow and contaminated snow, for which these assumptions are not critical. At glacier scale, our modeling approach based on a comparison between various impurity contents of surface snow and based on theoretical considerations regarding incident solar radiation, or surface conditions (melting or not) cannot provide accurate results

TCD
7, 6001–6042, 2013

on the effect of impurities on glacier melting but it is still useful to roughly quantify it, at least for the debris-free ablation zone.

Further investigations should be conducted to test these assumptions. Simulations using the detailed snow model Crocus (Vionnet et al., 2012) and reanalysis for past meteorological forcing can be done to investigate the effect of snow metamorphism and local meteorological conditions. Remote sensing data such as images from the imager MODIS can be used to infer the daily radiative forcing due to impurities (Dumont et al., 2012; Painter et al., 2012) and its spatial distribution over the Mera Glacier.

5 Conclusions

In this study, a 20 m firn core extracted from Mera Glacier in Nepal was used to reconstruct 10 yr of aerosol deposition fluxes at 6376 m on the southern flank of the Himalaya. Some species, like water stable isotopes, rBC, ammonium or fluoride deposition are consistent with the precipitation patterns related to the monsoon, with higher or spiking concentration during the dry season. rBC concentration were compared with BC atmospheric measurements from NCO-P station, both agrees for the timing but at different concentration levels in accord with the altitude difference between the sites. Other proxy, like dust revealed high and constant fluxes all over the year. These preliminary glaciochemical profiles quality and the in glacial temperature divulge that this site is a good candidate for environmental and climatic reconstruction based on ice core studies.

Dust and rBC aerosols present on the snow surface increase the potential snow melting by increasing the surface albedo. With this study using aerosol fluxes reconstructed from Mera Glacier firn core analyzes integrated by atmospheric measurements at the Nepal Climate Observatory – Pyramid, we estimate their impact on glacier melting. The analyzes reveal that mass fluxes are a few orders of magnitude higher for dust ($10.2 \pm 2.5\,g\,m^{-2}\,yr^{-1}$) than for rBC ($3.2 \pm 1.2\,mg\,m^{-2}\,yr^{-1}$), and that their deposition is distributed evenly over the year for dust but centered around pre-monsoon for rBC

TCD
7, 6001–6042, 2013

when wally wind breeze transport Atmospheric Brown Cloud pollutants accumulated over Himalayan foothills and North Indo-gangetic Plains up to Himalaya glaciers. Nevertheless, rBC concentrations, and than modeling applications, seem to be more representative of regional and large scale transport, while the dust flux at Mera Glacier is probably influenced by a strong local source. When compared in terms of fluxes, over this 10 yr time span, the variability in the ice core signal is rather reflecting the variability of the monsoon signal than that of emission intensity in the India+ area. According to aerosol concentrations reconstructed for the snow surface between 2000 and 2011, and using a modeling approach to calculate their impact on snow albedo and additional energy absorption, we estimated after several assumptions the potential melting induced by these impurities. Under some assumptions (surface concentration evolution, meteorological and snow surface conditions), the potential annual melting (10 yr mean values) generated by joint dust and rBC can reach $+662\,kg\,m^{-2}\,yr^{-1}$, with $+214\,kg\,m^{-2}\,yr^{-1}$ for rBC only. The comparison with direct mass balance measurements that provide ablation point-mass balance values of about $2280\,kg\,m^{-2}\,yr^{-1}$ around the equilibrium at 5400 m a.s.l. for the 2009–2010 period, and with melting derived from energy balance modeling ($4300\,kg\,m^{-2}\,yr^{-1}$), reveal that the estimated contribution of rBC alone to glacier melting is not more than 7 % and that the joint contribution of dust and rBC of the surface melting represents a maximum 18 % contribution to melting rate.

The impurities concentrations were measured only from one point in the accumulation area, based on an ice core. The next field campaign, in November 2013, will provide information on these dust and rBC concentration from much more spots on the glacier, in the accumulation area, for different altitude and orientation, but also from the ablation area where impurities can be concentrated or washed out on the ice surface.

Our results correspond to simulations based on last decade aerosol concentrations and fluxes, but what was the situation in the past? rBC is in majority produced by anthropogenic activities and its concentration increased highly over the last few decades, but what about past dust emission? Important questions are still open, and we will

TCD
7, 6001–6042, 2013

combine experimental and modeling approaches in the frame of the HIMICE project to reconstruct the past atmospheric composition in Northern India using Himalayan ice core records.

Acknowledgements. This work has been supported by the French Service d'Observation GLACIOCLIM, the French National Research Agency through ANR-09-CEP-005-01/PAPRIKA, and internal LGGE funding. We thank the porters who have been involved in field trips and coring operation, the Ev-K2-CNR and their Nepalese technicians for the assistance at the NCO-P.

The publication of this article is financed by CNRS-INSU.

References

Araguás-Araguás, L., Froehlich, K., and Rozanski, K.: Stable isotope composition of precipitation over southeast Asia, J. Geophys. Res., 103, 28721–28742, doi:10.1029/98jd02582, 1998.

Balkanski, Y., Schulz, M., Claquin, T., and Guibert, S.: Reevaluation of Mineral aerosol radiative forcings suggests a better agreement with satellite and AERONET data, Atmos. Chem. Phys., 7, 81–95, doi:10.5194/acp-7-81-2007, 2007.

Bonasoni, P., Laj, P., Marinoni, A., Sprenger, M., Angelini, F., Arduini, J., Bonafè, U., Calzolari, F., Colombo, T., Decesari, S., Di Biagio, C., di Sarra, A. G., Evangelisti, F., Duchi, R., Facchini, MC., Fuzzi, S., Gobbi, G. P., Maione, M., Panday, A., Roccato, F., Sellegri, K., Venzac, H., Verza, GP., Villani, P., Vuillermoz, E., and Cristofanelli, P.: Atmospheric Brown Clouds in the Himalayas: first two years of continuous observations at the Nepal Climate Observatory-Pyramid (5079 m), Atmos. Chem. Phys., 10, 7515–7531, doi:10.5194/acp-10-7515-2010, 2010.

TCD
7, 6001–6042, 2013

Bond, T. C., Bhardwaj, E., Dong, R., Jogani, R., Jung, S., Roden, C., Streets, D. G., and Trautmann, N. M.: Historical emissions of black and organic carbon aerosol from energy-related combustion, 1850–2000, Global Biogeochem. Cy., 21, GB2018, doi:10.1029/2006gb002840, 2007.

Bookhagen, B. and Burbank, D. W.: Topography, relief, and TRMM-derived rainfall variations along the Himalaya, Geophys. Res. Lett., 33, L08405, doi:10.1029/2006gl026037, 2006.

Cristofanelli, P., Bracci, A., Sprenger, M., Marinoni, A., Bonafè, U., Calzolari, F., Duchi, R., Laj, P., Pichon, J.M., Roccato, F., Venzac, H., Vuillermoz, E., and Bonasoni, P.: Tropospheric ozone variations at the Nepal Climate Observatory-Pyramid (Himalayas, 5079 m a.s.l.) and influence of deep stratospheric intrusion events, Atmos. Chem. Phys., 10, 6537–6549, doi:10.5194/acp-10-6537-2010, 2010.

Cross, E. S., Onasch, T. B., Ahern, A., Wrobel, W., Slowik, J. G., Olfert, J., Lack, D. A., Massoli, P., Cappa, C. D., Schwarz, J. P., Spackman, J. R., Fahey, D. W., Sedlacek, A., Trimborn, A., Jayne, J. T., Freedman, A., Williams, L. R., Ng, N. L., Mazzoleni, C., Dubey, M., Brem, B., Kok, G., Subramanian, R., Freitag, S., Clarke, A., Thornhill, D., Marr, L. C., Kolb, C. E., Worsnop, D. R., and Davidovits, P.: Soot particle studies "Instrument Inter-Comparison" project overview, Aerosol Sci. Tech., 44, 592–611, doi:10.1080/02786826.2010.482113, 2010.

Decesari, S., Facchini, M. C., Carbone, C., Giulianelli, L., Rinaldi, M., Finessi, E., Fuzzi, S., Marinoni, A., Cristofanelli, P., Duchi, R., Bonasoni, P., Vuillermoz, E., Cozic, J., Jaffrezo, J. L., and Laj, P.: Chemical composition of PM_{10} and PM_1 at the high-altitude Himalayan station Nepal Climate Observatory-Pyramid (NCO-P) (5079 m a.s.l.), Atmos. Chem. Phys., 10, 4583–4596, doi:10.5194/acp-10-4583-2010, 2010.

Delmonte, B., Petit, J., and Maggi, V.: Glacial to Holocene implications of the new 27000-year dust record from the EPICA Dome C (East Antarctica) ice core, Clim. Dynam., 18, 647–660, doi:10.1007/s00382-001-0193-9, 2002.

Diehl, T., Heil, A., Chin, M., Pan, X., Streets, D., Schultz, M., and Kinne, S.: Anthropogenic, biomass burning, and volcanic emissions of black carbon, organic carbon, and SO_2 from 1980 to 2010 for hindcast model experiments, Atmos. Chem. Phys. Discuss., 12, 24895–24954, doi:10.5194/acpd-12-24895-2012, 2012.

Dumont, M., Gardelle, J., Sirguey, P., Guillot, A., Six, D., Rabatel, A., and Arnaud, Y.: Linking glacier annual mass balance and glacier albedo retrieved from MODIS data, The Cryosphere, 6, 1527–1539, doi:10.5194/tc-6-1527-2012, 2012.

TCD
7, 6001–6042, 2013

Flanner, M. G., Liu, X., Zhou, C., Penner, J. E., and Jiao, C.: Enhanced solar energy absorption by internally-mixed black carbon in snow grains, Atmos. Chem. Phys., 12, 4699–4721, doi:10.5194/acp-12-4699-2012, 2012.

Fowler, D., Pilegaard, K., Sutton, M. A., Ambus, P., Raivonen, M., Duyzer, J., Simpson, D., Fagerli, H., Fuzzi, S., Schjoerring, J. K., Granier, C., Neftel, A., Isaksen, I. S. A., Laj, P., Maione, M., Monks, P. S., Burkhardt, J., Daemmgen, U., Neirynck, J., Personne, E., Wichink-Kruit, R., Butterbach-Bahl, K., Flechard, C., Tuovinen, J. P., Coyle, M., Gerosa, G., Loubet, B., Altimir, N., Gruenhage, L., Ammann, C., Cieslik, S., Paoletti, E., Mikkelsen, T. N., Ro-Poulsen, H., Cellier, P., Cape, J. N., Horva¡th, L., Loreto, F., Niinemets, Ã., Palmer, P. I., Rinne, J., Misztal, P., Nemitz, E., Nilsson, D., Pryor, S., Gallagher, M. W., Vesala, T., Skiba, U., Bruggemann, N., Zechmeister-Boltenstern, S., Williams, J., O'Dowd, C., Facchini, M. C., de Leeuw, G., Flossman, A., Chaumerliac, N., and Erisman, J. W.: Atmospheric composition change: ecosystems–atmosphere interactions, Atmos. Environ., 43, 5193–5267, doi:10.1016/j.atmosenv.2009.07.068, 2009.

Gautam, R., Hsu, N. C., Lau, W. K. M., and Yasunari, T. J.: Satellite observations of desert dust-induced Himalayan snow darkening, Geophys. Res. Lett., 40, 988–993, doi:10.1002/grl.50226, 2013.

Ginot, P., Kull, C., Schwikowski, M., Schotterer, U., and Gäggeler, H. W.: Effects of post-depositional processes on snow composition of a subtropical glacier (Cerro Tapado, Chilean Andes), J. Geophys. Res., 106, 32375–32386, 2001.

Ginot, P., Stampfli, F., Stampfli, D., Schwikowski, M., and Gäggeler, H. W.: FELICS, a new ice core drilling system for high-altitude glaciers, Fifth International Workshop on Ice Drilling Technology, Special Issue 56, 38–48, 2002.

Gobbi, G. P., Angelini, F., Bonasoni, P., Verza, G. P., Marinoni, A., and Barnaba, F.: Sun-photometry of the 2006–2007 aerosol optical/radiative properties at the Himalayan Nepal Climate Observatory-Pyramid (5079 m a.s.l.), Atmos. Chem. Phys., 10, 11209–11221, doi:10.5194/acp-10-11209-2010, 2010.

Granier, C., Bessagnet, B., Bond, T., D'Angiola, A., Denier van der Gon, H., Frost, G. J., Heil, A., Kaiser, J. W., Kinne, S., Klimont, Z., Kloster, S., Lamarque, J.-F., Liousse, C., Masui, T., Meleux, F., Mieville, A., Ohara, T., Raut, J.-C., Riahi, K., Schultz, M. G., Smith, S. J., Thompson, A., Aardenne, J., Werf, G. R., and Vuuren, D. P.: Evolution of anthropogenic and biomass burning emissions of air pollutants at global and regional scales during the 1980–2010 period, Clim. Change, 109, 163–190, doi:10.1007/s10584-011-0154-1, 2011.

TCD
7, 6001–6042, 2013

Hindman, E. E. and Upadhyay, B. P.: Air pollution transport in the Himalayas of Nepal and Tibet during the 1995–1996 dry season, Atmos. Environ., 36, 727–739, 2002.
International Atomic Energy Agency/World Meteorological Organization, I. W.: Global Network of Isotopes in Precipitation: The GNIP Database, Vienna (Austria), 2006.
Isaksen, I. S. A., Granier, C., Myhre, G., Berntsen, T. K., Dalsøren, S. B., Gauss, M., Klimont, Z., Benestad, R., Bousquet, P., Collins, W., Cox, T., Eyring, V., Fowler, D., Fuzzi, S., Jackel, P., Laj, P., Lohmann, U., Maione, M., Monks, P., Prevot, A. S. H., Raes, F., Richter, A., Rognerud, B., Schulz, M., Shindell, D., Stevenson, D. S., Storelvmo, T., Wang, W. C., van Weele, M., Wild, M., and Wuebbles, D.: Atmospheric composition change: climate–chemistry interactions, Atmos. Environ., 43, 5138–5192, doi:10.1016/j.atmosenv.2009.08.003, 2009.
Kang, S., Mayewski, P. A., Qin, D., Yan, Y., Hou, S., Zhang, D., Ren, J., and Kreutz, K.: Glacio-chemical records from a Mt. Everest ice core: relationship to atmospheric circulation over Asia, Atmos. Environ., 36, 3351–3361, 2002.
Kaspari, S., Mayewski, P. A., Handley, M., Osterberg, E., Kang, S., Sneed, S., Hou, S., and Qin, D.: Recent increases in atmospheric concentrations of Bi, U, Cs, S and Ca from a 350-year Mount Everest ice core record, J. Geophys. Res., 114, D04302, doi:10.1029/2008jd011088, 2009.
Kaspari, S. D., Schwikowski, M., Gysel, M., Flanner, M. G., Kang, S., Hou, S., and Mayewski, P. A.: Recent increase in black carbon concentrations from a Mt. Everest ice core spanning 1860–2000 AD, Geophys. Res. Lett., 38, L04703, doi:10.1029/2010gl046096, 2011.
Lamarque, J.-F., Bond, T. C., Eyring, V., Granier, C., Heil, A., Klimont, Z., Lee, D., Liousse, C., Mieville, A., Owen, B., Schultz, M. G., Shindell, D., Smith, S. J., Stehfest, E., Van Aardenne, J., Cooper, O. R., Kainuma, M., Mahowald, N., McConnell, J. R., Naik, V., Riahi, K., and van Vuuren, D. P.: Historical (1850–2000) gridded anthropogenic and biomass burning emissions of reactive gases and aerosols: methodology and application, Atmos. Chem. Phys., 10, 7017–7039, doi:10.5194/acp-10-7017-2010, 2010.
Lee, K., Hur, S. D., Hou, S., Burn-Nunes, L. J., Hong, S., Barbante, C., Boutron, C. F., and Rosman, K. J. R.: Isotopic signatures for natural versus anthropogenic pb in high-altitude mt. Everest ice cores during the past 800 years, Sci. Total Environ., 412–413, 194–202, doi:10.1016/j.scitotenv.2011.10.002, 2011.

TCD
7, 6001–6042, 2013

Libois, Q., Picard, G., France, J. L., Arnaud, L., Dumont, M., Carmagnola, C. M., and King, M. D.: Grain shape influence on light extinction in snow, The Cryosphere Discuss., 7, 2801–2843, doi:10.5194/tcd-7-2801-2013, 2013.

Lim, S., Cozic, J., Faïn, X., Zanatta, M., Jaffrezo, J. L., Ginot, P., and Laj, P.: Optimizing measurement methodology of refractory black carbon concentration in snow and ice and intercomparison with elemental carbon measurement method, Atmos. Meas. Tech. Discuss., submitted, 2013.

Lu, Z., Zhang, Q., and Streets, D. G.: Sulfur dioxide and primary carbonaceous aerosol emissions in China and India, 1996–2010, Atmos. Chem. Phys., 11, 9839–9864, doi:10.5194/acp-11-9839-2011, 2011.

Marcq, S., Laj, P., Roger, J. C., Villani, P., Sellegri, K., Bonasoni, P., Marinoni, A., Cristofanelli, P., Verza, G. P., and Bergin, M.: Aerosol optical properties and radiative forcing in the high Himalaya based on measurements at the Nepal Climate Observatory-Pyramid site (5079 m a.s.l.), Atmos. Chem. Phys., 10, 5859–5872, doi:10.5194/acp-10-5859-2010, 2010.

Marinoni, A., Polesello, S., Smiraglia, C., and Valsecchi, S.: Chemical composition of fresh-snow samples from the southern slope of Mt. Everest region (Khumbu-Himal region, Nepal), Atmos. Environ., 35, 3183–3190, 2001.

Marinoni, A., Cristofanelli, P., Laj, P., Duchi, R., Calzolari, F., Decesari, S., Sellegri, K., Vuillermoz, E., Verza, G. P., Villani, P., and Bonasoni, P.: Aerosol mass and black carbon concentrations, a two year record at NCO-P (5079 m, Southern Himalayas), Atmos. Chem. Phys., 10, 8551–8562, doi:10.5194/acp-10-8551-2010, 2010.

Menon, S., Koch, D., Beig, G., Sahu, S., Fasullo, J., and Orlikowski, D.: Black carbon aerosols and the third polar ice cap, Atmos. Chem. Phys., 10, 4559–4571, doi:10.5194/acp-10-4559-2010, 2010.

Ming, J., Zhang, D., Kang, S., and Tian, W.: Aerosol and fresh snow chemistry in the East Rongbuk Glacier on the northern slope of Mt. Qomolangma (Everest), J. Geophys. Res., 112, D15307, doi:10.1029/2007JD008618, 2007.

Ming, J., Cachier, H., Xiao, C., Qin, D., Kang, S., Hou, S., and Xu, J.: Black carbon record based on a shallow Himalayan ice core and its climatic implications, Atmos. Chem. Phys., 8, 1343–1352, doi:10.5194/acp-8-1343-2008, 2008.

Ming, J., Xiao, C., Cachier, H., Qin, D., Qin, X., Li, Z., and Pu, J.: Black Carbon (BC) in the snow of glaciers in west China and its potential effects on albedos, Atmos. Res., 92, 114–123, 2009.

TCD
7, 6001–6042, 2013

Moteki, N. and Kondo, Y.: Effects of mixing state on black carbon measurements by laser-induced incandescence, Aerosol Sci. Tech., 41, 398–417, doi:10.1080/02786820701199728, 2007.
Moteki, N. and Kondo, Y.: Dependence of laser-induced incandescence on physical properties of black carbon aerosols: measurements and theoretical interpretation, Aerosol Sci. Tech., 44, 663–675, doi:10.1080/02786826.2010.484450, 2010.
Painter, T. H., Bryant, A. C., and Skiles, S. M.: Radiative forcing by light absorbing impurities in snow from MODIS surface reflectance data, Geophys. Res. Lett., 39, L17502, doi:10.1029/2012gl052457, 2012.
Petzold, A. and Schönlinner, M.: Multi-angle absorption photometry – a new method for the measurement of aerosol light absorption and atmospheric black carbon, J. Aerosol Sci., 35, 421–441, doi:10.1016/j.jaerosci.2003.09.005, 2004.
Petzold, A., Ogren, J. A., Fiebig, M., Laj, P., Li, S.-M., Baltensperger, U., Holzer-Popp, T., Kinne, S., Pappalardo, G., Sugimoto, N., Wehrli, C., Wiedensohler, A., and Zhang, X.-Y.: Recommendations for reporting "black carbon" measurements, Atmos. Chem. Phys., 13, 8365–8379, doi:10.5194/acp-13-8365-2013, 2013.
Prasad, A. K. and Singh, R. P.: Changes in aerosol parameters during major dust storm events (2001–2005) over the Indo-Gangetic Plains using AERONET and MODIS data, J. Geophys. Res.-Atmos., 112, D09208, doi:10.1029/2006jd007778, 2007.
Preunkert, S. and Legrand, M.: Towards a quasi-complete reconstruction of past atmospheric aerosol load and composition (organic and inorganic) over Europe since 1920 inferred from Alpine ice cores, Clim. Past, 9, 1403–1416, doi:10.5194/cp-9-1403-2013, 2013.
Ricchiazzi, P., Yang, S., Gautier, C., and Sowle, D.: SBDART: a research and teaching software tool for plane-parallel radiative transfer in the Earth's atmosphere, B. Am. Meteorol. Soc., 79, 2101–2114, 1998.
Schwarz, J. P., Gao, R. S., Fahey, D. W., Thomson, D. S., Watts, L. A., Wilson, J. C., Reeves, J. M., Darbeheshti, M., Baumgardner, D. G., Kok, G. L., Chung, S. H., Schulz, M., Hendricks, J., Lauer, A., Kärcher, B., Slowik, J. G., Rosenlof, K. H., Thompson, T. L., Langford, A. O., Loewenstein, M., and Aikin, K. C.: Single-particle measurements of midlatitude black carbon and light-scattering aerosols from the boundary layer to the lower stratosphere, J. Geophys. Res.-Atmos., 111, D16207, doi:10.1029/2006jd007076, 2006.
Sellegri, K., Laj, P., Venzac, H., Boulon, J., Picard, D., Villani, P., Bonasoni, P., Marinoni, A., Cristofanelli, P., and Vuillermoz, E.: Seasonal variations of aerosol size distributions based on

TCD
7, 6001–6042, 2013

long-term measurements at the high altitude Himalayan site of Nepal Climate Observatory-Pyramid (5079 m), Nepal, Atmos. Chem. Phys., 10, 10679–10690, doi:10.5194/acp-10-10679-2010, 2010.
Shrestha, A. B., Wake, C. P., Dibb, J. E., and Whitlow, S. I.: Aerosol and precipitation chemistry at a remote Himalayan site in Nepal, Aerosol Sci. Tech., 36, 441–456, 2002.
Stamnes, K., Tsay, S. C., Wiscombe, W., and Jayaweera, K.: Numerically stable algorithm for discrete-ordinate-method radiative transfer in multiple scattering and emitting layered media, Appl. Optics, 27, 2502–2509, 1988.
Sterle, K. M., McConnell, J. R., Dozier, J., Edwards, R., and Flanner, M. G.: Retention and radiative forcing of black carbon in eastern Sierra Nevada snow, The Cryosphere, 7, 365–374, doi:10.5194/tc-7-365-2013, 2013.
Sun, J., Qin, D., Mayewski, P. A., Dibb, J. E., Whitlow, S., Li, Z., and Yang, Q.: Soluble species in aerosol and snow and their relationship at Glacier 1, Tien Shan, China, J. Geophys. Res.-Atmos., 103, 20021–20028, 1998.
Thompson, L. G., Mosley-Thompson, E., Davis, M. E., Bolzan, J. F., Dai, J., Klein, L., Yao, T., Wu, X., Xie, Z., and Gundestrup, N.: Holocene-late Pleistocene climatic ice core records from Qinghai-Tibetan plateau, Science, 246, 474–477, doi:10.1126/science.246.4929.474, 1989.
Thompson, L. G., Mosley-Thompson, E., Davis, M. E., Bolzan, J. F., Dai, J., Klein, L., Gundestrup, N., Yao, T., Wu, X., and Xie, Z.: Glacial stage ice core records from the subtropical Dunde ice cap, China, Ann. Glaciol., 14, 288–297, 1990.
Thompson, L. G., Yao, T., Mosley-Thompson, E., Davis, M. E., Henderson, K. A., and Lin, P. N.: A high-resolution millenial record of the South Asian monsoon from Himalayan ice cores, Science, 289, 1916–1919, 2000.
Ueno, K., Toyotsu, K., Bertolani, L., and Tartari, G.: Stepwise onset of monsoon weather observed in the Nepal Himalaya, Mon. Weather Rev., 136, 2507–2522, doi:10.1175/2007mwr2298.1, 2008.
van der Werf, G. R., Randerson, J. T., Giglio, L., Collatz, G. J., Kasibhatla, P. S., and Arellano Jr., A. F.: Interannual variability in global biomass burning emissions from 1997 to 2004, Atmos. Chem. Phys., 6, 3423–3441, doi:10.5194/acp-6-3423-2006, 2006.
Vionnet, V., Brun, E., Morin, S., Boone, A., Faroux, S., Le Moigne, P., Martin, E., and Willemet, J.-M.: The detailed snowpack scheme Crocus and its implementation in SURFEX v7.2, Geosci. Model Dev., 5, 773–791, doi:10.5194/gmd-5-773-2012, 2012.

TCD
7, 6001–6042, 2013

Vuille, M., Werner, M., Bradley, R. S., and Keimig, F.: Stable isotopes in precipitation in the Asian monsoon region, J. Geophys. Res., 110, D23108, doi:10.1029/2005jd006022, 2005.
Wagnon, P., Vincent, C., Arnaud, Y., Berthier, E., Vuillermoz, E., Gruber, S., Ménégoz, M., Gilbert, A., Dumont, M., Shea, J. M., Stumm, D., and Pokhrel, B. K.: Seasonal and annual mass balances of Mera and Pokalde glaciers (Nepal Himalaya) since 2007, The Cryosphere, 7, 1769–1786, doi:10.5194/tc-7-1769-2013, 2013.
Warren, S. G. and Brandt, R. E.: Optical constants of ice from the ultraviolet to the microwave: a revised compilation, J. Geophys. Res.-Atmos., 113, D14220, doi:10.1029/2007jd009744, 2008.
Warren, S. G. and Wiscombe, W. J.: A model for the spectral albedo of snow. II: Snow containing atmospheric aerosols, J. Atmos. Sci., 37, 2734–2745, 1980.
Xu, J., Hou, S., Qin, D., Kaspari, S., Mayewski, P. A., Petit, J.-R., Delmonte, B., Kang, S., Ren, J., Chappellaz, J., and Hong, S.: A 108.83-m ice-core record of atmospheric dust deposition at Mt. Qomolangma (Everest), Central Himalaya, Quaternary Res., 73, 33–38, 2010.
Yasunari, T. J., Bonasoni, P., Laj, P., Fujita, K., Vuillermoz, E., Marinoni, A., Cristofanelli, P., Duchi, R., Tartari, G., and Lau, K. M.: Estimated impact of black carbon deposition during pre-monsoon season from Nepal Climate Observatory – Pyramid data and snow albedo changes over Himalayan glaciers, Atmos. Chem. Phys., 10, 6603–6615, doi:10.5194/acp-10-6603-2010, 2010.
Yasunari, T. J., Tan, Q., Lau, K. M., Bonasoni, P., Marinoni, A., Laj, P., Ménégoz, M., Takemura, T., and Chin, M.: Estimated range of black carbon dry deposition and the related snow albedo reduction over Himalayan glaciers during dry pre-monsoon periods, Atmos. Environ., 78, 259–267, doi:10.1016/j.atmosenv.2012.03.031, 2013.
Zhang, Q., Kang, S., Kaspari, S., Li, C., Qin, D., Mayewski, P. A., and Hou, S.: Rare earth elements in an ice core from Mt. Everest: seasonal variations and potential sources, Atmos. Res., 94, 300–312, 2009.
Zhang, X., Masayoshi, N., Fujita, K., Yao, T., and Han, J.: Variation of precipitation $\delta^{18}O$ in Langtang Valley Himalayas, Sci. China Ser. D, 44, 769–778, doi:10.1007/bf02907089, 2001.

TCD
7, 6001–6042, 2013

Table 1. Data summary: EOF analyzes parameters and aerosol concentration and fluxes.

		All/Annual	Inter-monsoon	Monsoon	Winter	
	Samples	276	67 (24 %)	188 (68 %)	21 (8 %)	
	Ice core	19.8 m	4.81 m	12.62 m	2.37 m	
		12.47 m weq	3.19 m weq	8.09 m weq	1.19 m weq	
PC1	Variance	34 %	32 %	32 %	48 %	
PC2	Variance	15 % (49 %)	18 % (50 %)	16 % (47 %)	18 % (66 %)	
PC3	Variance	11 % (61 %)	14 % (65 %)	12 % (59 %)	12 % (79 %)	
$\delta^{18}O$	Mean composition	-17.21 ± 2.95	-13.92 ± 2.56	-17.75 ± 1.80	-21.98 ± 1.11	(‰)
NH_4^+	Mean concentration	1.69 ± 0.84	2.49 ± 0.96	1.55 ± 0.49	0.32 ± 0.15	($\mu Eq\,L^{-1}$)
F^-	Mean concentration	0.070 ± 0.060	0.120 ± 0.094	0.056 ± 0.026	0.026 ± 0.015	($\mu Eq\,L^{-1}$)
Ca^{2+}	Mean concentration	4.55 ± 2.80	5.81 ± 3.43	4.11 ± 2.34	4.36 ± 3.20	($\mu Eq\,L^{-1}$)
SO_4^{2-}	Mean concentration	1.05 ± 1.30	1.53 ± 1.60	0.87 ± 1.12	1.08 ± 1.37	($\mu Eq\,L^{-1}$)
NO_3^-	Mean concentration	1.08 ± 0.97	1.96 ± 1.30	0.80 ± 0.62	0.66 ± 0.37	($\mu Eq\,L^{-1}$)
rBC	Max. concentration	47.90	47.90	8.22	1.20	($\mu g\,L^{-1}$)
	Mean concentration	3.00	9.25	1.06	0.35	($\mu g\,L^{-1}$)
	Deposition flux	3.2 ± 1.2	($75\,\% \pm 12\,\%$)	($25\,\% \pm 12\,\%$)		($mg\,m^{-2}\,yr^{-1}$)
Dust	Max. concentration	66.9	66.9	26.5	15.4	($mg\,L^{-1}$)
	Mean concentration	10.1	11.1	10.1	6.5	($mg\,L^{-1}$)
	Deposition flux	10.1 ± 2.5	($28\,\% \pm 11\,\%$)	($72\,\% \pm 11\,\%$)		($g\,m^{-2}\,yr^{-1}$)

TCD
7, 6001–6042, 2013

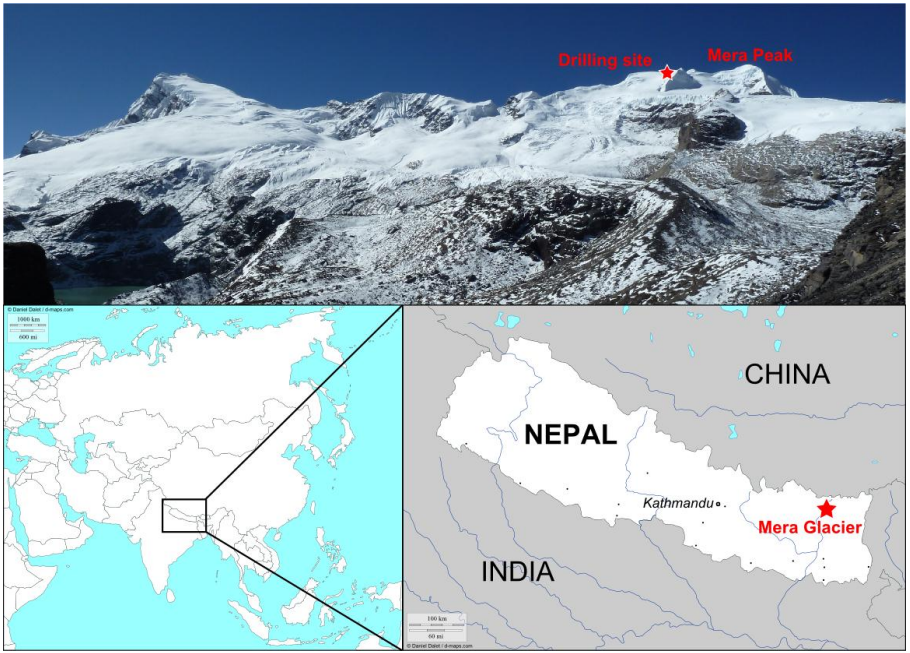

Fig. 1. Location of Mera Glacier in Nepal. The picture shows Mera Glacier view from the north and the drilling site position.

TCD
7, 6001–6042, 2013

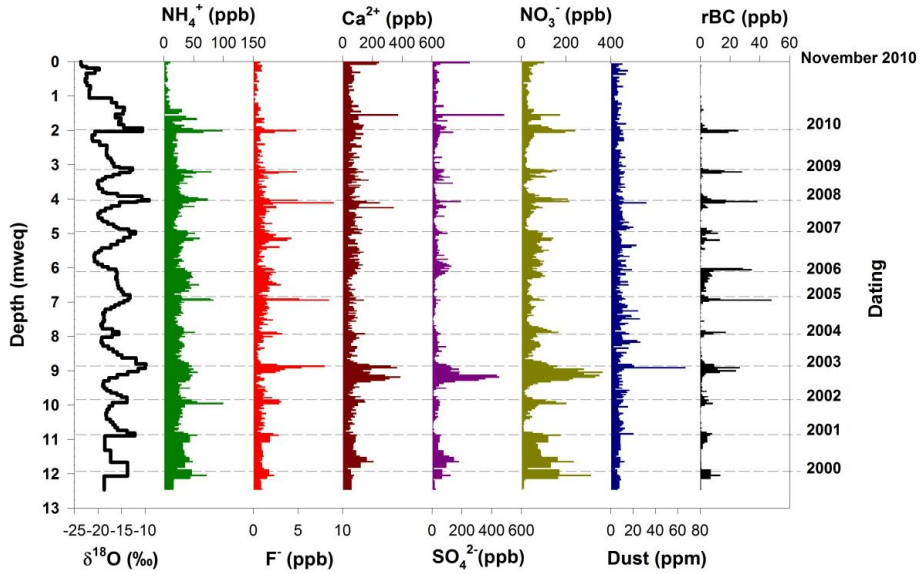

Fig. 2. Mera Glacier firn core profiles with depth for water stable isotope ($\delta^{18}O$), ammonium, fluoride, calcium, sulfate, nitrate, dust and refractory black carbon (rBC). The right vertical scale years corresponds to the annual dry season.

TCD
7, 6001–6042, 2013

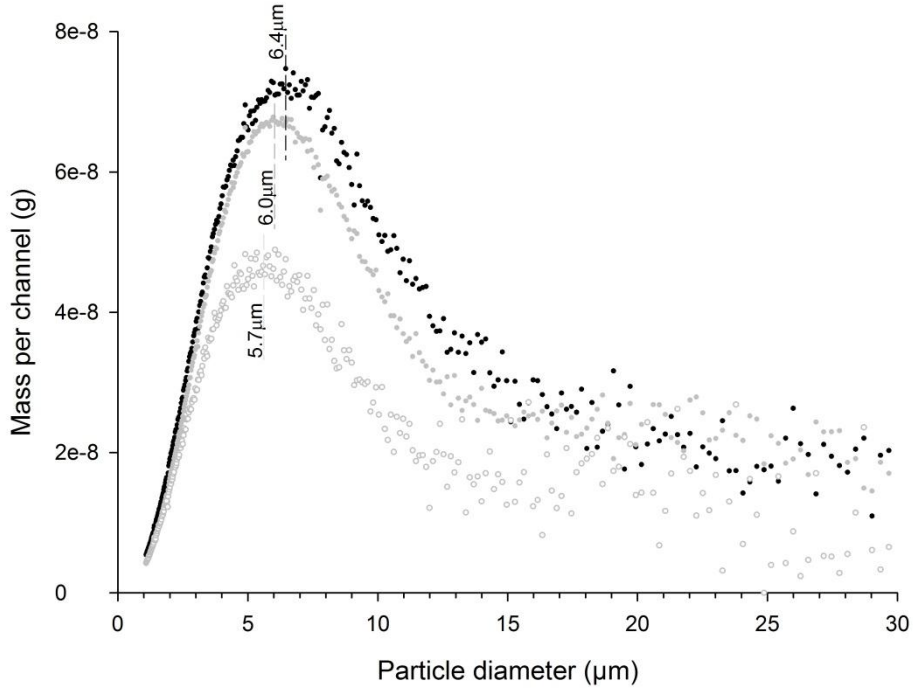

Fig. 3. Dust size distribution for the different season: inter-monsoon (black), monsoon (dark grey) and winter (white).

TCD
7, 6001–6042, 2013

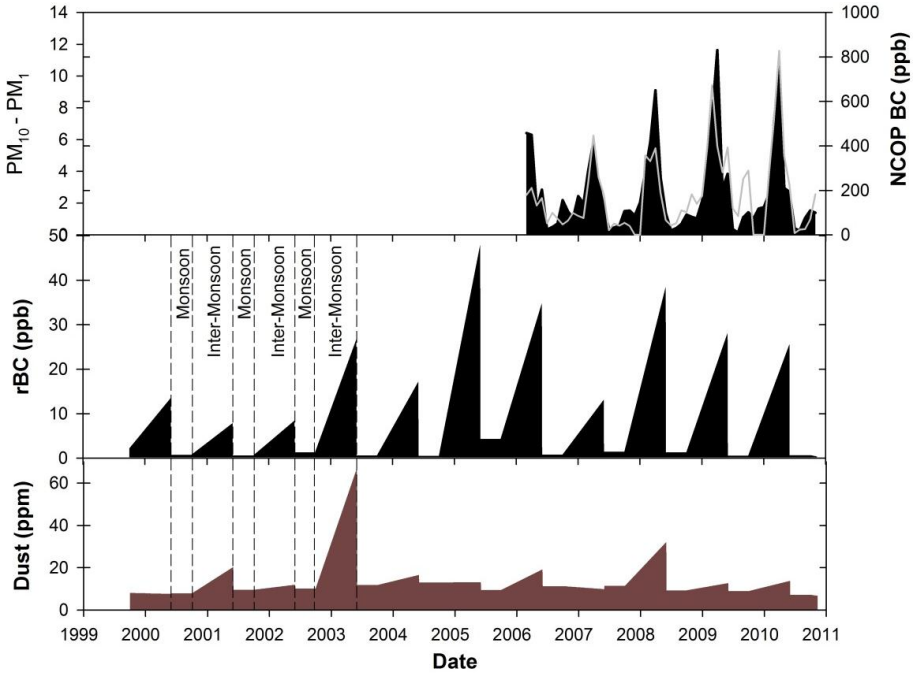

Fig. 4. Atmospheric BC (black) and dust (grey line) measured monthly at NCO-P station (top), and surface snow concentration evolution for rBC (black bar) and dust (drown bar) simulated from firn core data.

TCD
7, 6001–6042, 2013

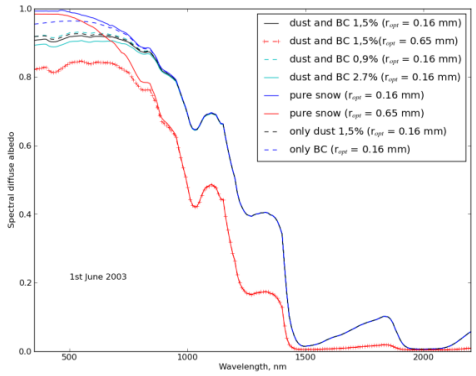

a)

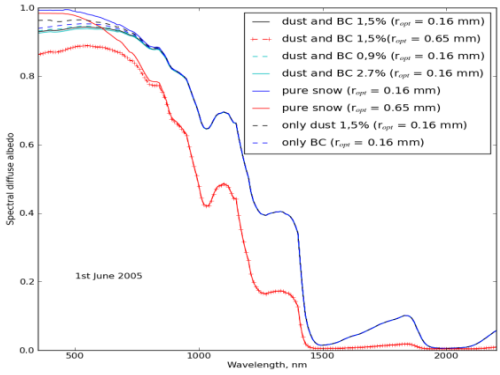

b)

Fig. 5. Simulated spectral albedo for the 1 June 2003 **(a)** and the 1 June 2005 **(b)**.

TCD
7, 6001–6042, 2013

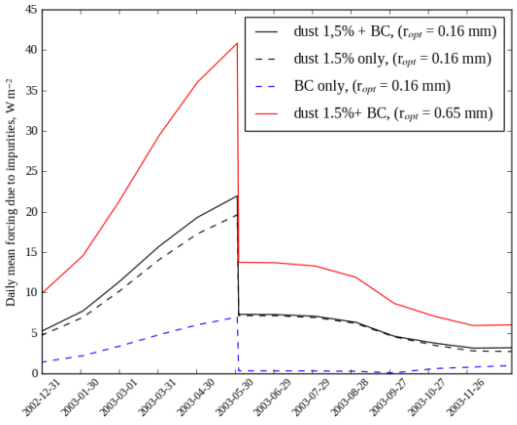

a)

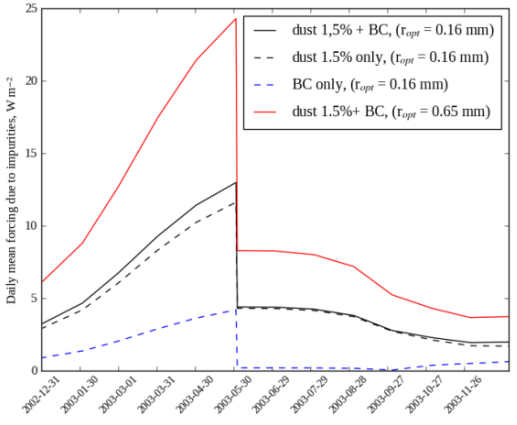

b)

Fig. 6. Daily mean forcing due to impurities **(a)** for clear sky **(b)** for cloudy sky for year 2003.

TCD
7, 6001–6042, 2013

A 10 yr record of black carbon and dust from Mera Peak ice core (Nepal)

P. Ginot et al.

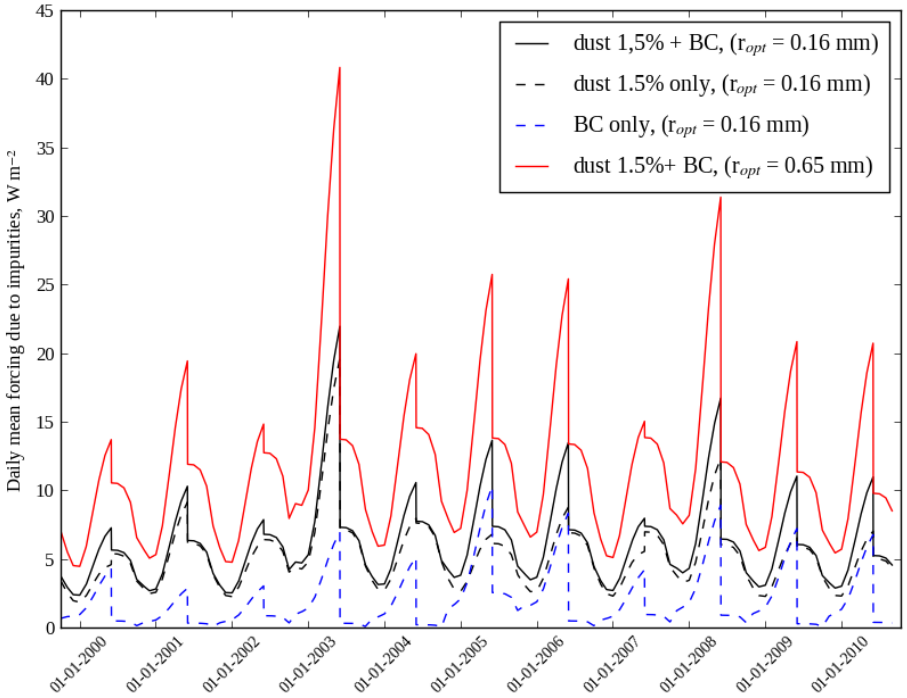

Fig. 7. Daily mean radiative forcing of impurity for clear sky simulation. The solid red and black lines are the additional energy due to the presence of dust and BC for coarse and fine snow. The black dotted line is for dust only and the blue dotted line is for BC only. The two solid lines are simulations for fine snow. For the results, the hematite content of dust is 1.5% as Balkanski et al. (2007), shows that the central content is around this value.

TCD
7, 6001–6042, 2013

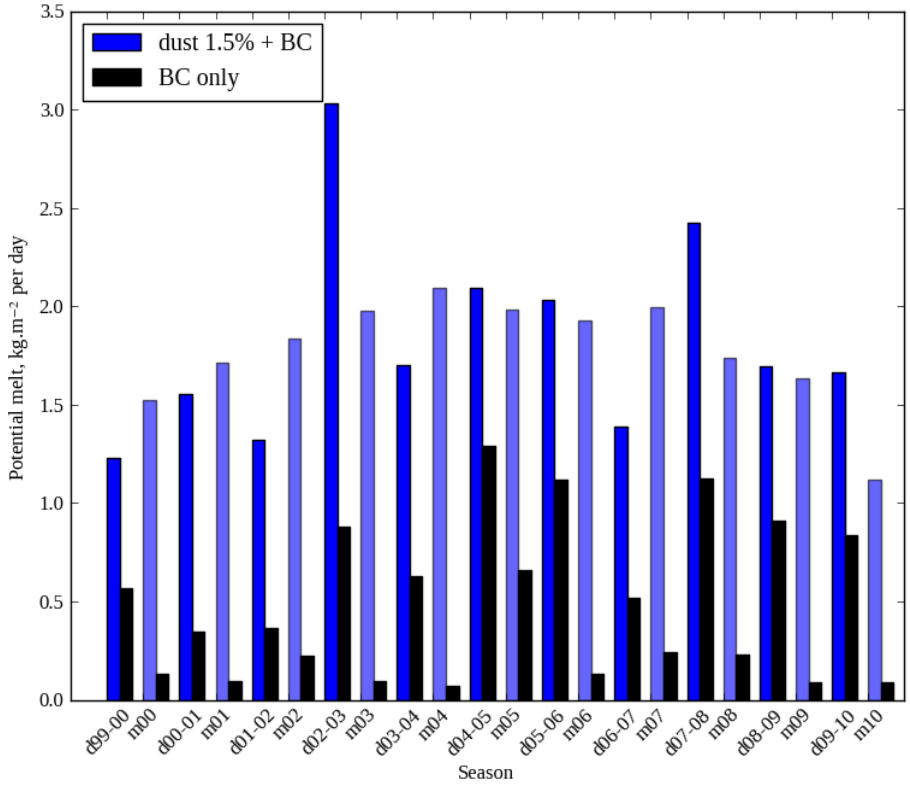

Fig. 8. Potential melt per day due to the presence of impurity in the snowpack for each dry (d) and monsoon (m) season of the study. The hematite content used is 1.5%. For each season, the first bar (blue) corresponds to the presence of both dust and BC, the second (black) to BC only.

TCD
7, 6001–6042, 2013